

Article

CO₂-Enhanced Radial Borehole Development of Shale Oil: Production Simulation and Parameter Analysis

Jiacheng Dai ^{1,2} , Kangjian Tian ¹, Zongan Xue ^{3,*} , Shuheng Ren ¹, Tianyu Wang ^{1,*}, Jingbin Li ^{1,2} and Shouceng Tian ¹

- ¹ National Key Laboratory of Petroleum Resources and Engineering, China University of Petroleum (Beijing), Beijing 102249, China; 2019310120@student.cup.edu.cn (J.D.); 2022210352@student.cup.edu.cn (K.T.); 2022010215@student.cup.edu.cn (S.R.); lij@cup.edu.cn (J.L.); tscsydx@cup.edu.cn (S.T.)
² Shaanxi Key Laboratory of Lacklustre Shale Gas Accumulation and Exploitation, Xi'an 717599, China
³ Oil & Gas Survey, China Geological Survey, Beijing 100083, China
* Correspondence: xuezhong@126.com (Z.X.); wangty@cup.edu.cn (T.W.)

Abstract: Shale oil resources, noted for their broad distribution and significant reserves, are increasingly recognized as vital supplements to traditional oil resources. In response to the high fracturing costs and swift decline in productivity associated with shale oil horizontal wells, this research introduces a novel approach utilizing CO₂ for enhanced shale oil recovery in radial boreholes. A compositional numerical simulation method is built accounted for component diffusion, adsorption, and non-Darcy flow, to explore the viability of this technique. The study examines how different factors—such as initial reservoir pressure, permeability, numbers of radial boreholes, and their branching patterns—influence oil production and CO₂ storage. Our principal conclusions indicate that with a constant CO₂ injection rate, lower initial reservoir pressures predominantly lead to immiscible oil displacement, hastening the occurrence of CO₂ gas channeling. Therefore, maintaining higher initial or injection pressures is critical for effective miscible displacement in CO₂-enhanced recovery using radial boreholes. Notably, the adsorption of CO₂ in shale oil results in the displacement of lighter hydrocarbons, an effect amplified by competitive adsorption. While CO₂ diffusion tends to prompt earlier gas channeling, its migration towards areas of lower concentration within the reservoir reduces the extent of channeling CO₂. Nonetheless, when reservoir permeability falls below 0.01 mD, the yield from CO₂-enhanced recovery using radial boreholes is markedly low. Hence, selecting high-permeability “sweet spot” regions within shale oil reservoirs for the deployment of this method is advisable. To boost oil production, utilizing longer and broader radial boreholes, increasing the number of boreholes, or setting the phase angle to 0° are effective strategies. Finally, by comparing the production of shale oil enhanced by CO₂ with that of a dual horizontal well fracturing system enhanced by CO₂, it was found that although the former’s oil production is only 50.6% of the latter, its cost is merely 11.1%, thereby proving its economic viability. These findings present a new perspective for the economically efficient extraction of shale oil, offering potential guidance for industrial practices.

Keywords: shale oil; radial borehole; CO₂-EOR; numerical simulation



Citation: Dai, J.; Tian, K.; Xue, Z.; Ren, S.; Wang, T.; Li, J.; Tian, S. CO₂-Enhanced Radial Borehole Development of Shale Oil: Production Simulation and Parameter Analysis. *Processes* **2024**, *12*, 116. <https://doi.org/10.3390/pr12010116>

Received: 12 November 2023
Revised: 14 December 2023
Accepted: 21 December 2023
Published: 2 January 2024



Copyright: © 2024 by the authors. Licensee MDPI, Basel, Switzerland. This article is an open access article distributed under the terms and conditions of the Creative Commons Attribution (CC BY) license (<https://creativecommons.org/licenses/by/4.0/>).

1. Introduction

The consumption rate of petroleum resources has been increasing in tandem with the pace of global economic development. A comparison of global petroleum consumption from 2015 to 2019 with that from 1970 to 1974 reveals an increase by a factor of 1.77, yet the addition of proven reserves has declined to 11.2% [1]. As the development of existing conventional oil fields enters the middle and late stages, and the difficulty in finding new conventional oil and gas resources intensifies, unconventional oil and gas resources have become an important substitute for oil and gas production [2]. Unconventional oil

and gas resources are abundant, with the world's recoverable unconventional oil and gas resources estimated at 442.1 billion tons and 227 trillion cubic meters, respectively [3]. Shale oil resources, as a significant component of unconventional oil and gas resources, have witnessed substantial yields. In 2018, the daily production of shale oil in the United States reached 6 million barrels, emanating from multiple basins including Eagle Ford, Spraberry, Bakken, and others [4]. China boasts rich terrestrial shale oil resources, with technically recoverable resources estimated at 4.393 billion tons, ranking among the world's largest in reserves. However, the characteristics of shale reservoirs include ultra-low permeability, micro- and nanoscale porosity, heterogeneity, and anisotropy [5–7], leading to an initial recovery rate for shale oil that is only between 7 and 15% [8,9].

The combination of horizontal wells and multi-stage hydraulic fracturing is the primary method for developing shale oil [10], where the creation of main hydraulic fractures and numerous micro-fractures in the reservoir forms the main channels for oil and gas flow, thus facilitating the commercial development of shale oil [11]. However, the cost of hydraulic fracturing technology for horizontal wells is relatively high, and the drilling and completion of a single horizontal well can exceed USD 10 million [12]. Moreover, hydraulic fracturing consumes a substantial amount of water; in most shale oil-producing areas in the United States, the water used for fracturing accounts for more than 70% of the total water consumption, with each well in the Eagleford region using up to 4.4 million gallons [13]. In shale oil reservoirs with high clay content, hydraulic fracturing can cause clay swelling, which decreases reservoir permeability [14]. In summary, current hydraulic fracturing technology does not meet the developmental needs of all shale oil reservoirs, thus prompting the need to explore new methods for the cost-effective development of shale oil reservoirs.

In the process of developing shale oil, it is often encountered that the rate of decline in oil production is rapid. Taking the average production statistics from the Eagleford area compiled by Henrick et al. as an example, if depletion production methods are employed, the output after 24 months of production declines to 14.8% of the initial value [15]. The decline in production during depletion is due to the gradual decrease in reservoir pressure. In conventional oil and gas resources, water injection is commonly used on-site to maintain reservoir pressure. However, the commercial application of water flooding in the development of shale oil reservoirs is not widespread [16]. This is because injected water does not reduce the viscosity of the crude oil, resulting in low injection rates and an inability to effectively maintain the pressure differential between injection and production wells. Due to the strong heterogeneity of shale oil reservoirs, there is a tendency for water breakthrough, leading to a limited sweep area during water flooding [17]. Moreover, the high content of clay minerals in some shale oil reservoirs can cause a water sensitivity effect upon water injection, reducing reservoir permeability. Sheng and Chen found through numerical simulation that the recovery rate by gas drive in hydraulically fractured shale oil reservoirs was 15.1%, whereas the recovery rate by water flooding was about 11.9% [18].

Hence, using CO₂ as an alternative medium to water for injection into shale oil reservoirs can not only enhance the recovery rate of shale oil, but also serve as an important method for carbon capture, utilization, and storage (CCUS) [19]. Currently, the sequestration of CO₂ in deep geological formations is the only technically feasible solution that ensures the continued use of fossil fuels while reducing CO₂ emissions [20,21]. In shale oil reservoirs, where temperatures and pressures are high, injected CO₂ can be maintained in a supercritical state. Supercritical CO₂ exhibits characteristics of high density similar to liquids, and low viscosity and high diffusivity similar to gases [22]. On the microscopic level, supercritical CO₂ (scCO₂) can more easily diffuse into nanoscale pores compared to water [23], and tends to adsorb onto the surfaces of microfine pores more than lighter hydrocarbon molecules [24]. The primary mechanisms of CO₂ Enhanced Oil Recovery (EOR) include the expansion of oil volume [25,26], reduction in viscosity [27], reduction in interfacial tension [28], and the extraction of light components [29–31]. From a macroscopic

perspective, once the pressure is above the minimum miscibility pressure, CO₂ can form a piston-like front, creating a more uniform displacement profile [29,32].

Inspired by the high cost of hydraulic fracturing and the enhanced oil recovery benefits of CO₂ injection, this paper proposes for the first time a new approach for CO₂-enhanced shale oil development using “vertical wells + radial boreholes”. As depicted in Figure 1, multiple hydraulically created radial boreholes are drilled in the upper and lower layers of a vertical well within the shale oil reservoir, with one layer serving as the CO₂ injection zone and the other as the oil production layer. This method can expand the flow range of shale oil and increase production per well on a single-well basis. The deployment of radial boreholes is flexible, allowing for the bypassing of interlayers; and the drilling and production costs of this method are significantly lower than those of hydraulic fracturing [33], making it a promising new method for the safe and efficient development of shale oil reservoirs. However, the effectiveness of the radial boreholes CO₂ EOR method in developing shale oil reservoirs remains to be verified. Reservoir numerical simulation methods have long been used to predict the flow dynamics of crude oil during CO₂ EOR and the subsurface storage dynamics of CO₂ [34,35], and are capable of analyzing a variety of wellbore configurations, including multi-lateral and fishbone wells [36,37]. Leveraging these research methodologies could enable the effective analysis of the dynamics of CO₂ EOR using radial boreholes.

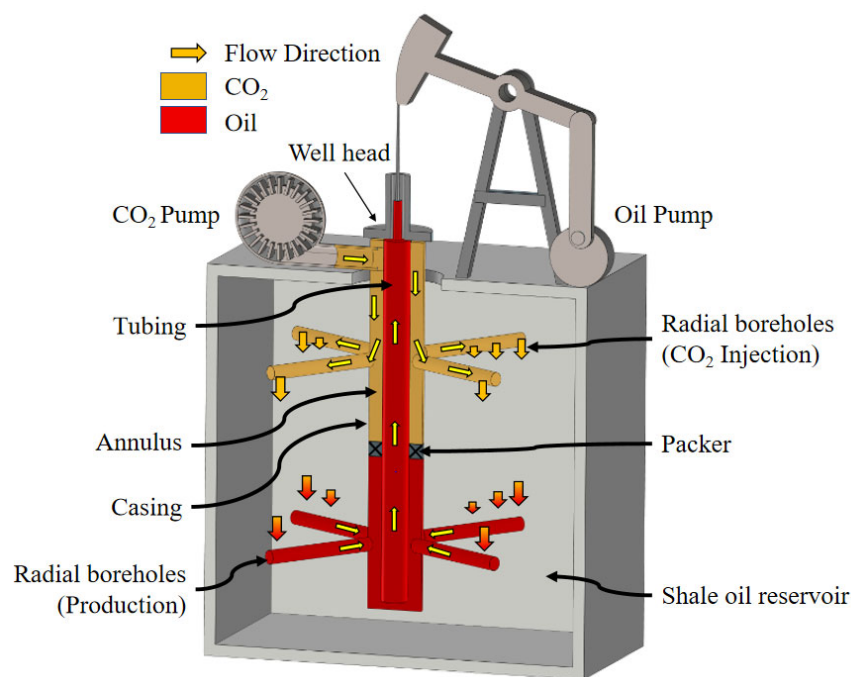


Figure 1. Diagram of CO₂-enhanced radial borehole shale oil production.

To study the feasibility of the method of CO₂-enhanced shale oil recovery in radial boreholes, a numerical simulation model of reservoir composition was established based on the parameters of Eagleford shale oil in the United States, taking into account the two geological parameters of initial reservoir pressure and formation permeability, the characteristics of shale reservoir with diffusion, adsorption and the non-Darcy effect, the radial length, and the radius of the borehole. The effects of four design parameters, branch number, and phase angle on oil production and CO₂ storage are assessed. The research results provide a new method and reference for the economic development of shale oil.

2. CO₂-Enhanced Radial Borehole Method

Radial jet drilling is a technique that employs a high-pressure jet drill to bore one or multiple small horizontal boreholes with radii of 20–50 mm and lengths of 10–100 m, distributed across single or multiple layers from a main wellbore [38]. Radial jet drilling

has made substantial technical breakthroughs in perforating near-well low-permeability areas, expanding the contact area of the reservoir, and bridging faults, fissures, and natural fractures with high permeability [39]. It is applied in reservoirs with low permeability, thin layers, fractured formations, “dead zones” after water injection, lithological inclusion deposits, exploratory wells, and development wells where fracturing results are poor, and in the vicinity of wells where severe formation damage and blockage occur [40].

This paper builds upon the foundation of radial jet drilling technology, and further proposes a method combining radial boreholes with CO₂ flooding for the development of shale oil. As shown in Figure 1, a vertical well is drilled into the shale oil reservoir, with two sets of radial boreholes drilled at both deep and shallow levels of the reservoir. Tubing is run to the bottom of the well, and packers are placed in the annulus between the upper and lower sets of radial boreholes. CO₂ is injected into the annulus, with the CO₂ driving the crude oil through the upper radial boreholes into the reservoir, causing it to flow downwards, and the oil then returns to the surface through the lower radial boreholes. This method does not require fracturing, has a simple procedure, and can achieve continuous production from a single well.

3. Numerical Model

3.1. Composition Model

During the process of CO₂ injection into shale oil reservoirs for oil displacement, the adsorption of CO₂, its diffusion, miscible/non-miscible driving between CO₂ and oil, as well as the non-Darcy flow of fluids are key mechanisms that cannot be ignored. Compared with the black oil model, the compositional model can more accurately describe the multiphase and multicomponent dynamics during the CO₂ flooding process, especially the diffusion and adsorption of various components [41]. Therefore, this paper has adopted the compositional model to simulate the process of CO₂ displacement via radial boreholes. Furthermore, to consider the miscible and non-miscible displacement in the reservoir, an overall compositional model was employed [42].

It is imperative to acknowledge that compositional models, though profoundly effective in simulating fluid behaviors within oil and gas reservoirs, encounter a spectrum of constraints. These models are marked by their computational complexity, necessitating substantial processing capabilities and extensive time investment, attributable to the multifaceted computations for various components across different phases. The fidelity of these models is significantly contingent on the employed equation of state, which may not invariably encapsulate the intricacies of complex mixtures or conditions at extreme parameters. A notable impediment arises from uncertainties in fluid characterization; inaccuracies in data acquisition can precipitate considerable deviations in the simulation outcomes. A further limitation is their tendency to overlook minute-scale heterogeneities within reservoirs, a consequence of their predilection for larger-scale analyses, which can engender inaccuracies, especially in reservoirs characterized by heterogeneity. Predominantly, these models presuppose an equilibrium in phase behavior, an assumption that may not consistently mirror the non-equilibrium dynamics prevalent in actual reservoir scenarios. The exigency for comprehensive and granular data sets further compounds the challenge, rendering these models acutely sensitive to input variables and necessitating meticulous calibration against empirical field data. Additionally, environmental contingencies, such as geomechanical alterations or chemical interactions, are not exhaustively integrated, potentially affecting the reservoir’s performance and the model’s prognostic precision. Despite these impediments, compositional models remain indispensable in reservoir engineering, offering nuanced insights into fluid dynamics. Nevertheless, these considerations fall outside the purview of this article. Future work will delve into the refinement and enhancement of compositional models in light of these identified limitations.

To optimize simulation convergence, it is assumed that the reservoir temperature remains isothermal throughout the process and is unaffected by the injection of CO₂; non-stimulated reservoir volume (non-SRV) areas effectively form closed reservoir boundaries

due to extremely low permeability; the water phase in the reservoir is not considered, hence the diffusion and dissolution of CO₂ in water, capillary pressure, the hysteresis effects of relative permeability, the nano-pore confinement effects, as well as the impacts of asphaltene and hydrate formation are all considered negligible.

For the oil and gas phases, considering diffusion and adsorption, the material balance equations can be formulated as [43,44]:

$$\partial_t [\phi \sum_{\alpha=o,g} \rho_{\alpha} S_{\alpha} X_{\alpha}^i + \delta_s (1 - \phi) \rho_s^i] + \sum_{\alpha=l,v} \nabla \cdot (\rho_{\alpha} X_{\alpha}^i \vec{v}_{\alpha} + J_{\alpha}^i) - \sum_{\alpha=o,g} \rho_{\alpha} X_{\alpha}^i q_{\alpha} / V = 0 \quad (1)$$

where the subscript i represents the component; the subscript α represents the phase (liquid or vapor); ρ represents density, kg/m³; S stands for the saturation, dimensionless; X represents the mass fraction, dimensionless; v is Darcy's velocity, m/s; δ_s is a logical parameter that is set to one in the shale matrix and zero elsewhere; τ is tortuosity, dimensionless; J stands for diffusion, m²/s, which is expressed by Fick's diffusion law as [45]

$$J_{\alpha}^i = -\frac{\phi S_{\alpha}}{\tau} D_{\alpha}^i \nabla (\rho_{\alpha} X_{\alpha}^i) \quad (2)$$

where ϕ is the matrix porosity, dimensionless; D stands for diffusion coefficient, m²/s.

ρ_s in Formula (1) represents the adsorption capacity when the pressure is P , kg/m³. When multiple components exist at the same time, it can be written according to the extended Langmuir formula [46]:

$$\rho_s^i = \rho_{sL}^i \frac{y_i \frac{P}{P_L}}{1 + \sum_{j=1}^n y_j \frac{P}{P_L}} \quad (3)$$

where ρ_{sL} represents the maximum adsorption quantity, measured in kg/m³, and P_L denotes the minimal pressure required to achieve this maximum adsorption capacity, Pa. The variable y corresponds to the molar fraction of components within the gas phase. It is important to acknowledge that utilizing the extended Langmuir equation to characterize adsorption phenomena in shale oil is a somewhat reductive approach. Currently, shale oil adsorption theories are still in a nascent phase, and there is a lack of appropriate models to accurately describe the competitive adsorption interactions between CO₂ and other components [47]. Thus, the enhancement of our understanding of competitive adsorption in shale oil components is earmarked for future research endeavors.

For the velocity–pressure differential relationship, this paper employs distinct non-Darcy laws for the gas and oil phases [48].

$$\vec{v}_{\alpha} = \frac{k_{r\alpha} K_0}{\mu_{\alpha}} \eta_{N\alpha} [\nabla P - \rho_{\alpha} g \nabla Z] \quad (4)$$

where $k_{r\alpha}$ denotes the relative permeability; K_0 indicates the absolute permeability, Darcy; μ_{α} stands for the viscosity, cp; g is the gravitational acceleration, set at 9.8 N/kg; Z is the depth, m; $\eta_{N\alpha}$ represents the non-Darcy coefficient for phase alpha and the liquid phase l ,

$$\eta_{NI} = \frac{1}{1 + a e^{-b|\nabla P|}} \quad (5)$$

where the coefficients a and b are functions of mobility. It should be noted that to ensure the value of a does not fall below zero when the mobility is high, adjustments have been made to the formula for a based on the original literature.

$$a = e^{-1.176(\frac{K_0 k_{rL}}{\mu_l})} \quad (6)$$

$$b = 0.3603 \left(\frac{K_0 k_{rl}}{\mu_l} \right)^2 - 0.1049 \left(\frac{K_0 k_{rl}}{\mu_l} \right) + 1.0935 \quad (7)$$

The mechanisms of gas transport in shale reservoirs vary based on the Knudsen number. When the Knudsen number is below 0.001, the continuum flow regime is dominant due to the prevalence of intermolecular collisions. As the Knudsen number increases to a range between 0.001 and 0.1, the frequency of molecular–wall collisions rises, leading to the occurrence of slip flow where slippage effects become significant. In situations where the Knudsen number lies between 0.1 and 10, the frequency of molecular–wall collisions becomes comparable to that of intermolecular collisions, resulting in the transitional flow regime. Finally, when the Knudsen number exceeds 10, molecular–wall collisions predominate, and the gas transport is characterized by Knudsen diffusion. This progression illustrates the transition from continuum flow to Knudsen diffusion as the Knudsen number increases, reflecting the changing dynamics of gas transport mechanisms [49]. According to the Beskok and Karniadakis (BK) model [50], the gas non-Darcy coefficient can be expressed as

$$\eta_{Nv} = \left(1 + \frac{4Kn}{1 + 4Kn} \right) \left(1 + \frac{128}{15\pi^2} Kn \cdot \tan^{-1} (4Kn^{0.4}) \right) \quad (8)$$

where Kn is the Knudsen number, which is defined as [51]

$$Kn = \frac{\lambda}{d} \quad (9)$$

where d represents the pore diameter, m. λ represents the molecular mean free path, m, which is defined as [52]

$$\lambda = \frac{\mu_v}{P_v} \sqrt{\frac{\pi RT}{2M}} \quad (10)$$

where μ_v is the dynamic viscosity of the vapor phase, Pa·s. R is the universal gas constant, which is 8.314 J/(mol·K). T is the temperature, Kelvin. M is the molecular molar mass, kg/mol.

The relationship between pore diameter, permeability, and porosity can be expressed as [53]:

$$d = 2\sqrt{2\tau} \sqrt{\frac{K_0}{\phi}} \quad (11)$$

This paper assumes no-flow boundary conditions, which are expressed as in reference [54]:

$$\vec{v}_\alpha \cdot \vec{n} = 0 \quad (12)$$

where n represents the normal vector belonging to the boundary.

In this study, the Peaceman wellbore model is adopted to address the connectivity between radial boreholes and the computational grid. The discretization of the spatial flux terms is implemented using the finite volume method coupled with two-point flux approximation. The discretization of the governing equations for flow in the matrix, wellbore, and fractures is accomplished through the Newton–Raphson iterative technique, culminating in a set of equations. Within this set, the current time step is indicated by $n + 1$, whereas n signifies the preceding time step. The term R_i denotes the residual for component i .

$$\frac{\partial R^{n+1}}{\partial Va} \Delta Va = -R^{n+1} \quad (13)$$

where the left-hand side is composed of the Jacobian matrix, and Va represents the initial variables; R is the residual. The MATLAB Reservoir Simulation Toolkit (MRST 2023a) is utilized in this study to solve Equation (13) [55,56].

This paper's vapor–liquid equilibrium was determined through the resolution of the Flash Problem using the Rachford–Rice method, and further characterized by the

physical properties of each phase as dictated by the Peng–Robinson equation of state. Given that different strategies for solving the coupled system of equations can significantly influence the nonlinear solution process, the Overall Composition Formulation method was employed to better resolve processes driven by multiphase flow. This formulation utilizes pressure and N-1 overall mole fractions as its primary variables. Detailed strategies for this solution approach can be found in reference [56]. The paper does not take into account capillary pressure.

3.2. CO₂-Enhanced Radial Borehole Model

This study situates a vertical well at the center of a reservoir with a 200 m radius and 50 m height. Schematic representations of two radial borehole configurations are illustrated in Figure 2. At depths of 12 m and 38 m, two layers of radial boreholes are installed, each comprising either two or four boreholes. For the two-boreholes configuration, the boreholes across both layers maintain no phase difference, while a 45° phase angle is set between layers in the four-boreholes configuration. The length and radius of the radial boreholes are 50 m and 50 mm, respectively. The boreholes in the same layer maintain consistent angular separation between each other. The vertical well is indirectly connected to the reservoir; fluids enter the radial boreholes and are gathered into the vertical well before flowing to the surface. In the primary scenario of this study, radial boreholes extend 30 m, with a diameter of 30 mm. The upper boreholes are designated for CO₂ injection and the lower for oil extraction, with injection and production pressures set at 66.02 MPa and 46.02 MPa, respectively, over a simulated production span of five years. Additional parameters within the reservoir are provided in Table 1.

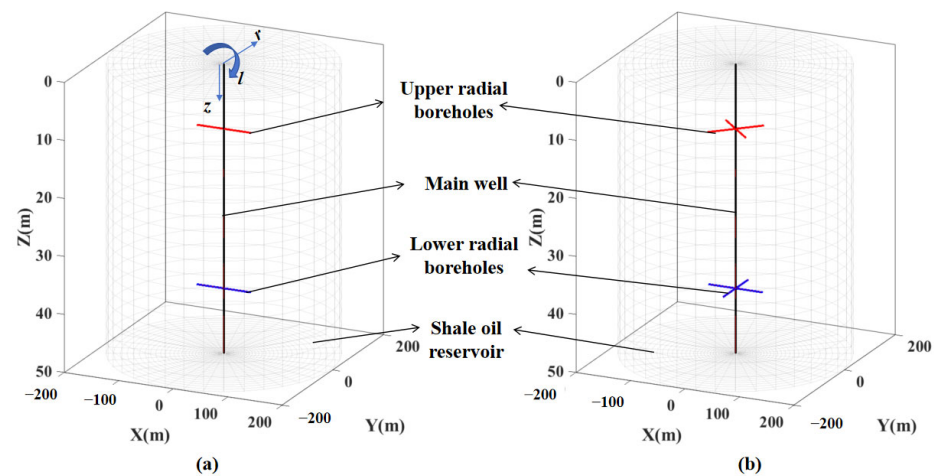


Figure 2. Schematic diagram of radial borehole: (a) 2 layer, 2 branch, 0° phase angle; (b) 2 layer, 4 branch, 45° phase angle. The arrows *l*, *r*, and *z*, respectively, represent the circumferential, radial, and vertical directions.

Table 1. Shale reservoir parameters.

Parameters	Value	Parameters	Value
Reservoir radius, m	200	Matrix compressibility, barsa	1×10^5
Reservoir thickness, m	50	Gas density (STP), kg/m ³	2.76
Tortuosity	2	Oil density (STP), kg/m ³	887.97
Reservoir pressure, MPa	56.02	Kr coefficient	2
Reservoir temp, K	405.372	Oil viscosity (underground), cp	0.8
Permeability, mD	0.1	Oil saturation, %	58

This research performed numerical simulations using parameters representative of the Eagle Ford shale play. The hydrocarbon fluid model comprises CO₂, N₂ and C₁, and

groups C₂-C₅, C₆-C₁₀, and C₁₁₊, forming six pseudo-components. The characteristics of these pseudo-components and their binary interaction parameters, essential for phase behavior calculations, are derived from the methodology proposed in reference [57].

Table 2 details the diffusion and adsorption coefficients for the pseudo-components. Notably, this study sets the Langmuir coefficients for CO₂, and components C₁ to C₆ from literature sources [46], while assumptions for the Langmuir coefficients of the heavier components beyond C₆ are based on solubility experiments [58].

Table 2. Shale oil component diffusion and adsorption parameters.

	CO ₂	N ₂	C ₁	C ₂ -C ₆	C ₆ -C ₁₀	C ₁₁₊
$D_i, 10^{-9} \text{ m}^2/\text{s}$	2.91	4.13	4.13	1.27	0.58	0.36
$P_L, \text{ MPa}$	5.76	12.41	10.76	5.82	2.07	1.38
$\rho_{SL}, \text{ kg}/\text{m}^3$	7.77	1.61	3.00	9.59	10.18	10.71

3.3. Model Validation

To verify the accuracy of the model, this paper initially employed experimental data derived from a radial constant volume diffusion device to validate the diffusion and adsorption accuracies. This device operates by placing shale oil samples saturated with oil in a CO₂ environment. Due to diffusion and adsorption effects, CO₂ migrates into the core, causing a drop in the environmental pressure. As illustrated in Figure 3, when the diffusion coefficient is small, the ability of CO₂ to penetrate the core weakens, hence the trend of environmental pressure decline over time diminishes. When the core's diffusion coefficient is around 10–11 m²/s, the results closely align with the experimental findings of Peng et al. [59], indicating the effectiveness of the diffusion and adsorption model. It is important to note that since there is no significant change in environmental pressure, adsorption has a minimal impact on the results. Additionally, the intensity of CO₂ diffusion in shale oil reservoirs remains not fully determined [57], thus this paper adopts larger numerical values to make the impact of diffusion more pronounced.

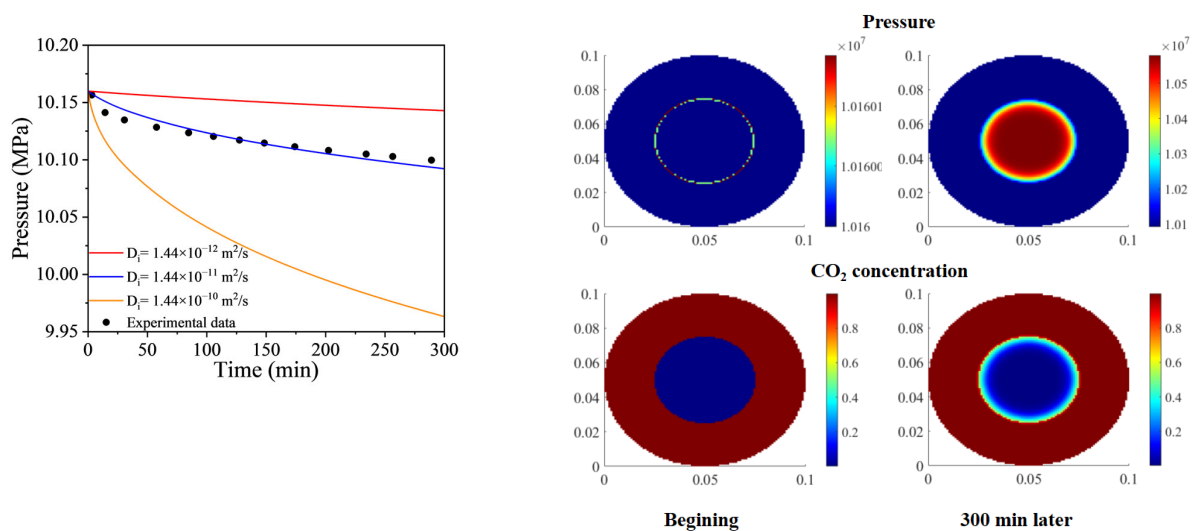


Figure 3. Comparison between experimental and simulated data for CO₂-shale radial constant volume diffusion.

For the non-Darcy law of liquids, the non-Darcy law proposed by Peng and Sheng has been widely applied and recognized, aligning with the adsorption layer theory in pipe flow. However, due to the heterogeneity of shale and complex flow mechanisms, it may not entirely fit the pressure drop to flow rate relationship, as illustrated. As shown in Figure 4, the Equation (5) shows some deviation in predicting core data compared to the

empirical data from Li et al. [60], though experimental values still distribute around the predicted data. When applying Equation (5), a pressure differential of around 2 MPa can cause an approximate 50% error in apparent permeability, leading to an underestimation of production, while a pressure differential exceeding 5 MPa might result in overestimation. In the cores used by Li et al., apparent permeability decreases under high pressure differentials. The authors suggest this phenomenon might be due to larger pores being accessible at higher pressures, increasing resistance. Currently, no mature model can fully explain this phenomenon. We plan to model this behavior in the future and analyze its impact on the CO₂-enhanced development of shale oil.

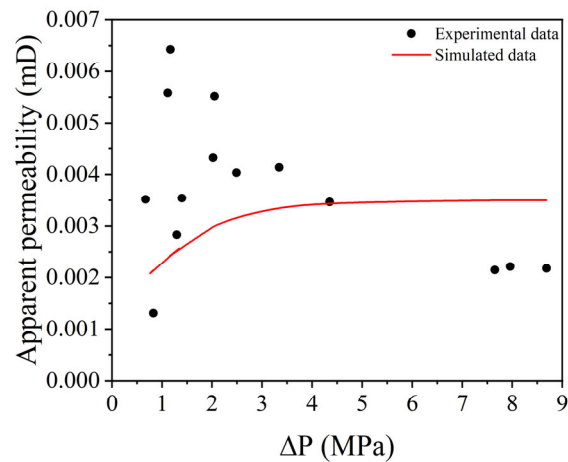


Figure 4. Comparison of liquid phase non-Darcy law with experimental test data.

For the non-Darcy law of gases, we employed the steady-state oil displacement analytical solution considering the Klinkenberg effect proposed by Wu et al. [7] and compared it with a numerical solution calculated under the same conditions. As depicted in Figure 5, our numerical model aligns well with the analytical solution, validating the accuracy of the non-Darcy gas transport law incorporating Knudsen diffusion. It should be noted that for both liquid and gas non-Darcy laws, multiple models exist. For instance, Xu et al. explored gas transport behavior in tapered elliptical and rectangular channels [49], finding that with an increase in taper ratio and aspect ratio, under a constant mean cross-sectional area, the average conductance of Knudsen diffusion and viscous flow decreases, while the average surface diffusion conductance initially increases and then decreases. Xu et al. [61] further discussed the impact of nano-scale pore size distributions on gas production. They found that a higher fractal dimension and a larger variance enhance gas flow in shale rocks due to a higher fraction of large pores, resulting in increased apparent permeability. In the future, we plan to refine our model based on physical simulations and field experiments.

In Section 4.1, based on a formation pressure of 60 MPa, we varied the number of circumferential grids (n_l), radial grids (n_r), and vertical grids (n_z), taking the bottom-hole pressure of the injection well as a reference. As shown in Figure 6, it was observed that the variations in n_l , n_r , and n_z become minimal when they exceed 36, 28, and 20, respectively. It is important to note that when altering the number of vertical grids, the relative positioning of the wellbore and the grids also impacts the changes in bottom-hole pressure. To optimize computational efficiency, this study selects 36, 28, and 20 as the respective values for n_l , n_r , and n_z .

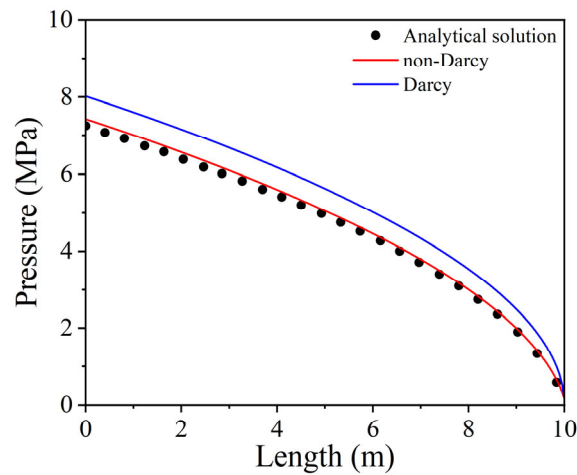


Figure 5. Comparison of gas phase non-Darcy law with analytical solutions.

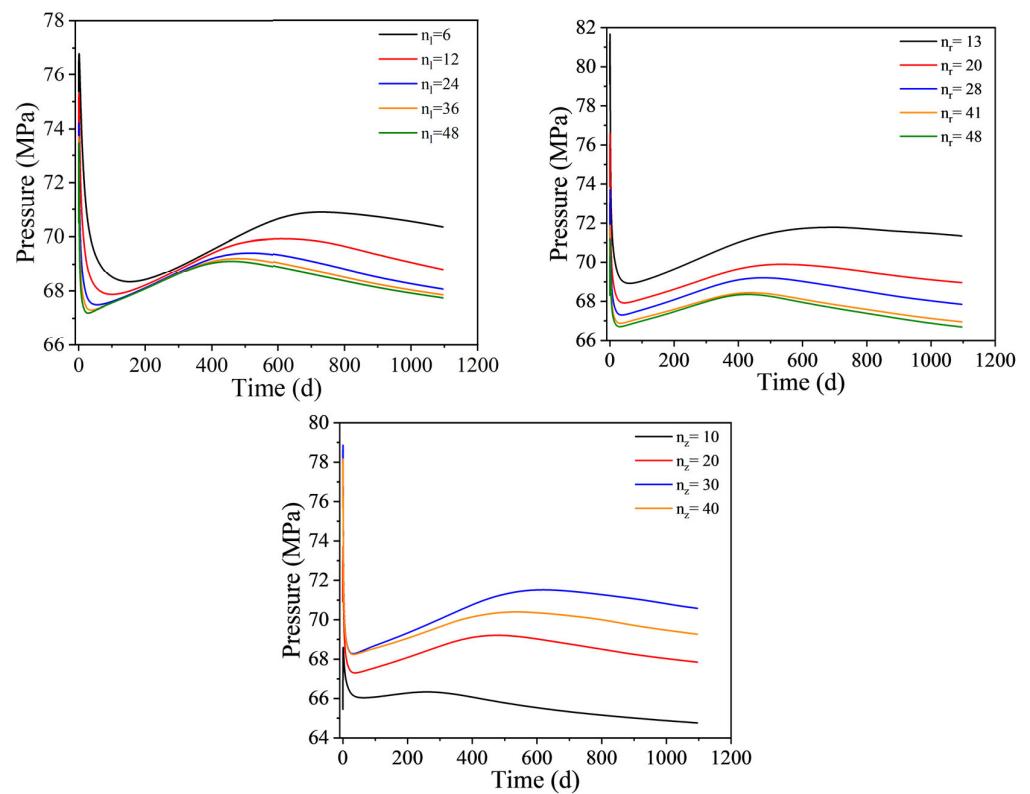


Figure 6. Validation of grid independence.

4. Results and Discussion

4.1. Effect of Initial Reservoir Pressure

Initial reservoir pressure is a critical factor in determining the miscibility of CO₂ and oil displacement. In this context, CO₂ surface injection rates were maintained at 5000 m³/day, with initial formation pressures set between 30 MPa and 60 MPa, matching the production well pressure to the initial formation pressure. It has been observed that lower reservoir pressures are more conducive to immiscible flooding in the CO₂-oil displacement process. In immiscible flooding scenarios, due to the viscosity differences between CO₂ and crude oil at the displacement front, CO₂ tends to channel more centrally, leading to a less uniform displacement profile. In contrast, miscible flooding eliminates the CO₂-crude oil interface, resulting in a more even, “piston-like” displacement pattern, as depicted in Figure 7.

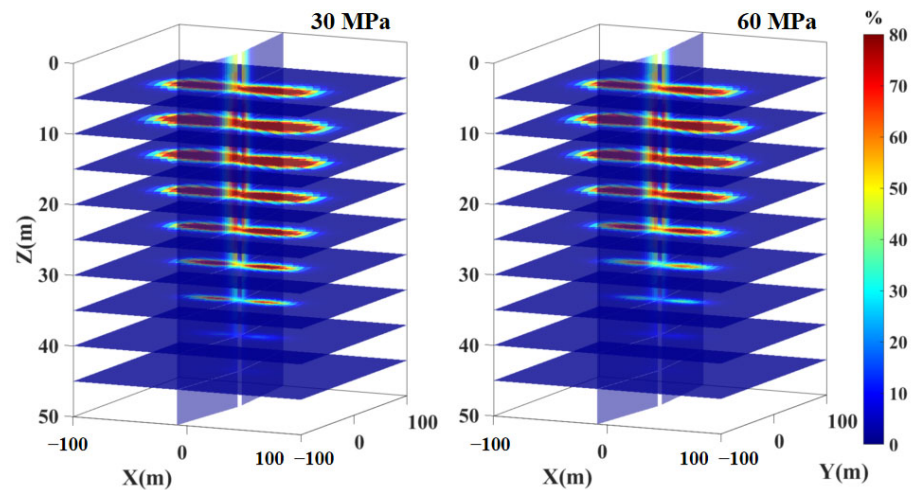


Figure 7. Spatial distribution of CO₂ mole fraction at varying initial reservoir pressures on day 600.

Additionally, at lower initial reservoir pressures, the mole fraction of CO₂ in the lower strata increases. This condition enhances the probability of gas channeling at the same CO₂ injection rate. For example, as demonstrated in Figure 8, with an initial reservoir pressure of 60 MPa, the onset of gas channeling was delayed by 120 days compared to a 30 MPa reservoir pressure. This delay in gas channeling at higher pressures also correlates with a slower decrease in CH₄ production, highlighting the significant impact of reservoir pressure on the dynamics and efficacy of CO₂-enhanced oil recovery methods.

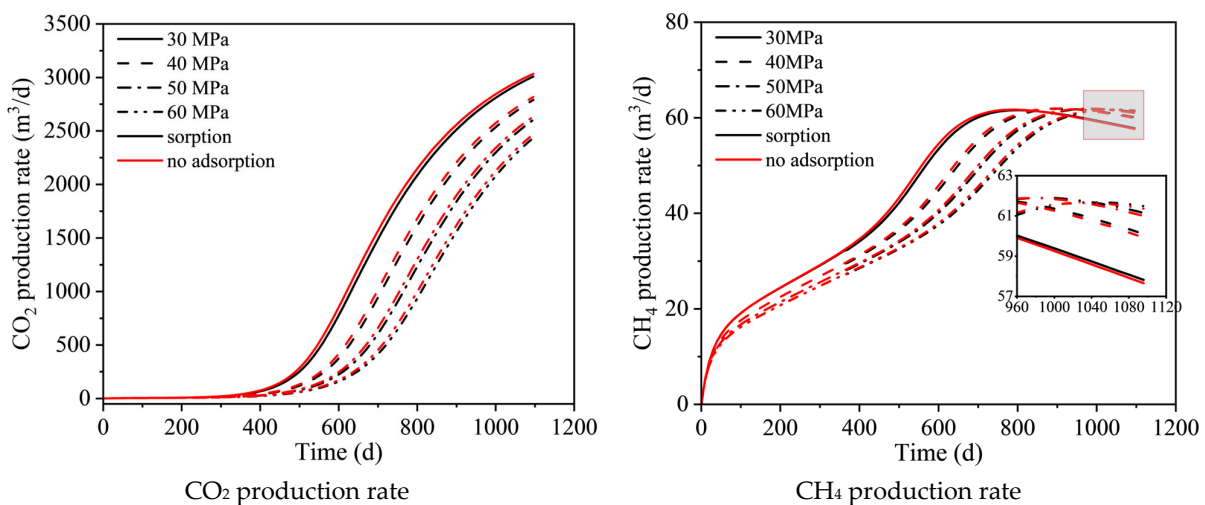


Figure 8. Temporal variation in CO₂ and CH₄ production rates under different initial reservoir pressures.

In scenarios where adsorption occurs, CO₂ production is observed to be lower compared to cases without adsorption, attributable to a portion of CO₂ being adsorbed within the reservoir matrix. Regarding CH₄, prior to gas channeling, a certain amount of CH₄ is adsorbed in the matrix, resulting in reduced CH₄ production compared to situations where adsorption is not a factor. However, the regions traversed by CO₂ experience desorption of the initially adsorbed CH₄, facilitated by competitive adsorption, thereby releasing more CH₄. Consequently, CH₄ production post-gas channeling, in the presence of adsorption, exceeds that observed in the absence of adsorption.

4.2. Effect of Permeability

Reservoir permeability is a key determinant of the fluid flow capacity within a reservoir. In this analysis, the initial formation pressure was set at 56.02 MPa, with the injection well pressure at 57.02 MPa, and the production well pressure at 55.02 MPa. Observations from Figures 9 and 10 suggest that with lower reservoir permeabilities, the injection of CO₂ becomes increasingly challenging, consequently impeding oil production. In Figure 10, the red dotted line represents the CO₂ storage rate when non-Darcy's law and diffusion are taken into account. Thus, it is advised to employ radial boreholes for shale oil development only when reservoir permeability exceeds 0.01 mD. Considering a permeability of 1 mD, there is an initial production phase (0–0.625 d) during which the reservoir pressure diminishes, triggering the release of elastic energy from rocks and fluids. This results in a rapid decline in production, ultimately reducing the production rate to 65% of its original value. Subsequently, as the reservoir pressure stabilizes (0.625 d–450 d), oil production gradually increases. However, post 220 d, both the gas storage rate and oil production rate start to decline due to CO₂ channeling. At lower permeability levels, significant gas channeling is not observed, as less CO₂ is injected within the same timeframe.

In the presence of non-Darcy flow, the flow capacity of the liquid phase is influenced by the permeability of the reservoir. As permeability decreases, the coefficient “a” in the relevant formula increases, leading to a higher value of η_{NI} and, consequently, a reduced flow capacity of the liquid phase. Conversely, lower permeability results in smaller matrix pore sizes, as inferred from Equation (11). This smaller pore size leads to a reduced value of K_n , as per the equation, and an increased value of η_{Ng} , according to Equation (8), implying an enhanced gas flow capacity with decreasing permeability. Figures 9 and 10 illustrate how these opposing effects neutralize each other, culminating in an overall reduction in production due to non-Darcy effects at low permeability levels. However, when permeability exceeds 1 mD, both η_{NI} and η_{Ng} approach 1, indicating that liquid and gas phases flow by Darcy's law. For instance, at permeabilities of 0.001 mD and 1 mD, the oil production rate in the third year under non-Darcy conditions is 0.98 and 0.99 times, respectively, of the rate under Darcy conditions. Notably, production characteristics typically associated with lower permeabilities can be observed in the early stages of production in higher-permeability contexts.

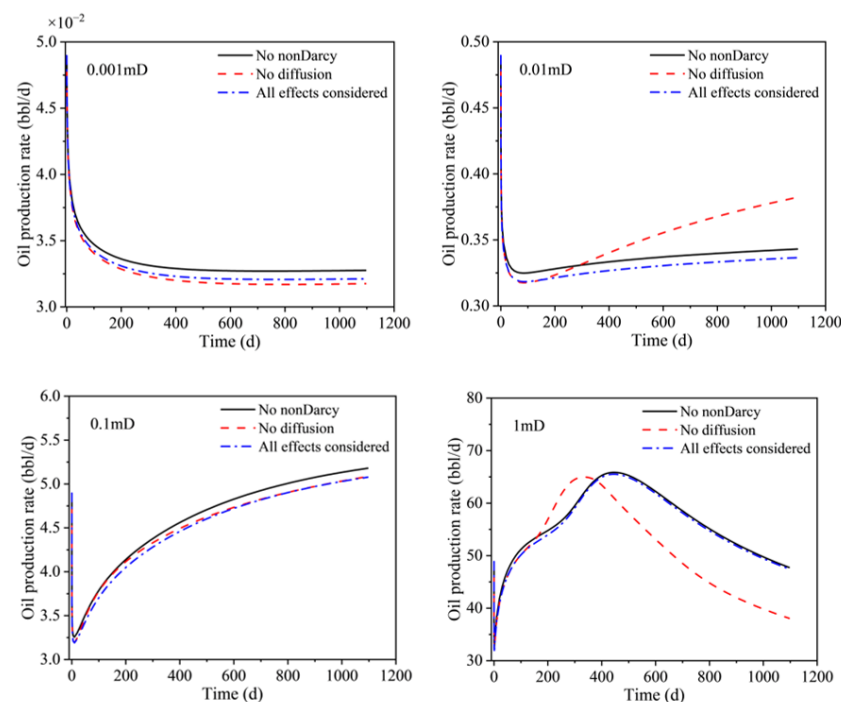


Figure 9. Temporal variation of oil production rate under different matrix permeability levels.

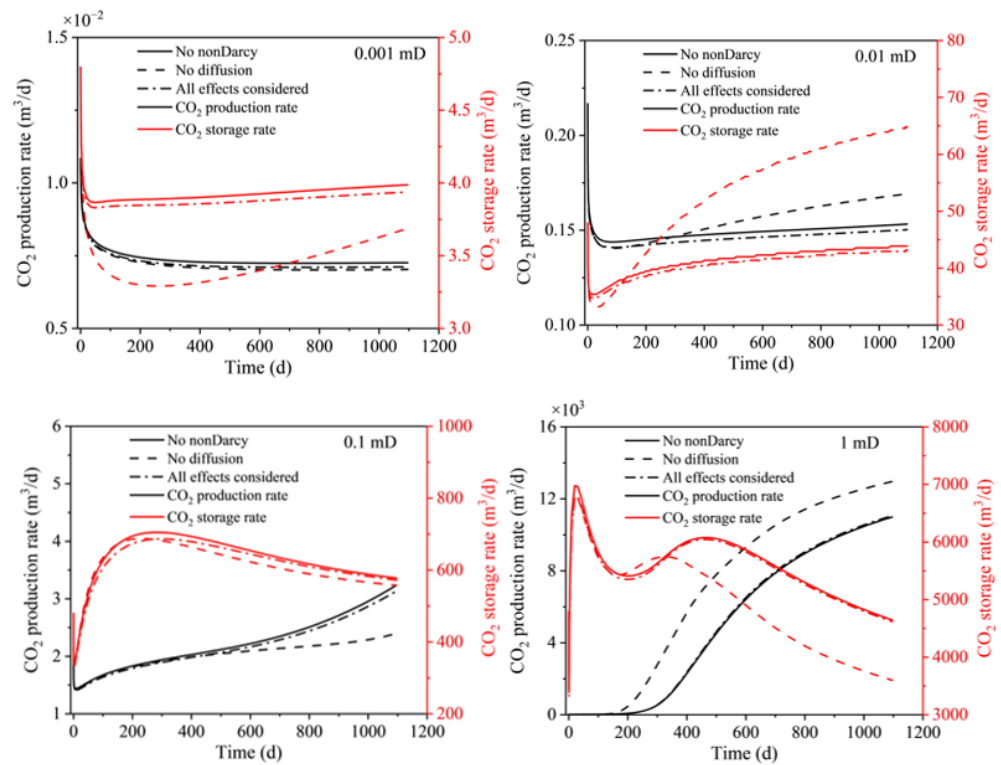


Figure 10. Temporal variation of CO₂ production rate and storage rate under different matrix permeability levels.

At a matrix permeability of 0.0001 mD, the reservoir's extreme density renders the pressure gradient insufficient to effectively drive oil and gas flow. Under these conditions, the diffusion of components emerges as a significant driving mechanism for the movement of both oil and CO₂. Consequently, if diffusion is not factored in, the rates of oil production, CO₂ production, and CO₂ storage are observed to be lower. It is crucial to clarify that the CO₂ production in this scenario refers to the CO₂ originally present in the reservoir, rather than the CO₂ that has been injected.

With a matrix permeability of 0.01 mD, the injected CO₂ predominantly accumulates around the injection radial boreholes, and fluid flow primarily occurs in the horizontal direction. In this scenario, the reservoir pressure has not yet reached a complete steady state. When diffusion is accounted for, CO₂ tends to flow more readily toward the reservoir boundary. This diffusion effect results in a smaller horizontal pressure gradient compared to the scenario where diffusion is not considered, as illustrated in Figure 11. Consequently, the CO₂ injection rate, when diffusion is not factored in, is marginally higher than the rate with diffusion considered. Similarly, the oil production rate is slightly higher when diffusion is taken into account compared to when it is not.

At a matrix permeability of 0.1 mD, the predominant direction of fluid flow transitions from horizontal to vertical as the reservoir pressure gradually stabilizes into a steady state. In such a scenario, the vertical pressure gradients, whether diffusion is considered or not, are equivalent. As a result, the oil production rates are essentially identical under both conditions. However, the diffusion effect of CO₂ leads to a more rapid vertical migration when diffusion is taken into account. This phenomenon is demonstrated in Figure 12. Therefore, when considering diffusion, the onset of CO₂ gas channeling occurs earlier compared to scenarios where diffusion is not factored in.

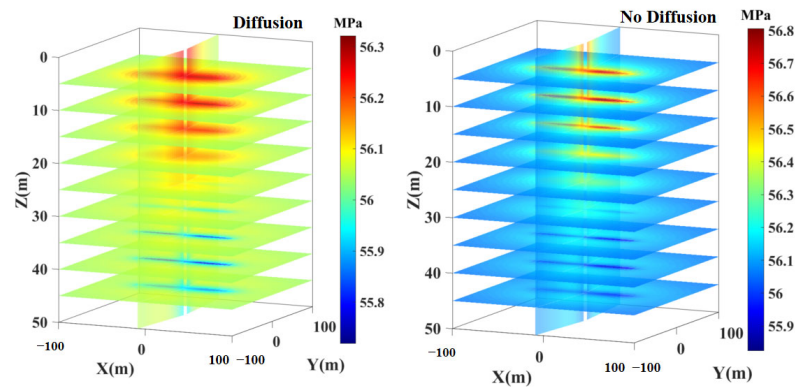


Figure 11. Reservoir pressure distribution in the third year when matrix permeability is 0.01 mD.

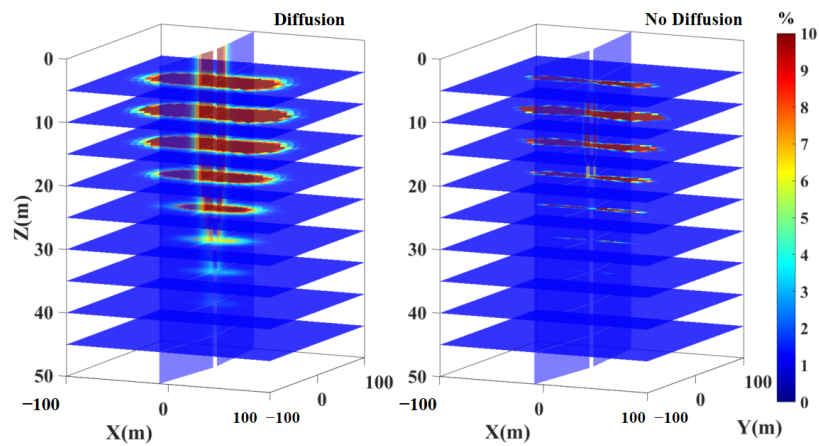


Figure 12. The molar fraction of CO₂ in the third year when the matrix permeability is 0.1 mD.

When the matrix permeability is set at 1 mD and component diffusion is present, CO₂ may channel earlier, but its migration is not confined solely to the production radial borehole under a pressure gradient. Instead, a portion of CO₂ also flows towards the reservoir boundary. This implies that the reservoir is more effective at retaining CO₂ when diffusion is considered. Consequently, the amount of CO₂ gas channeling is substantially lower compared to in scenarios where diffusion is not taken into account, as shown in Figure 13. Additionally, oil production begins to decline approximately 120 days later than in cases without diffusion.

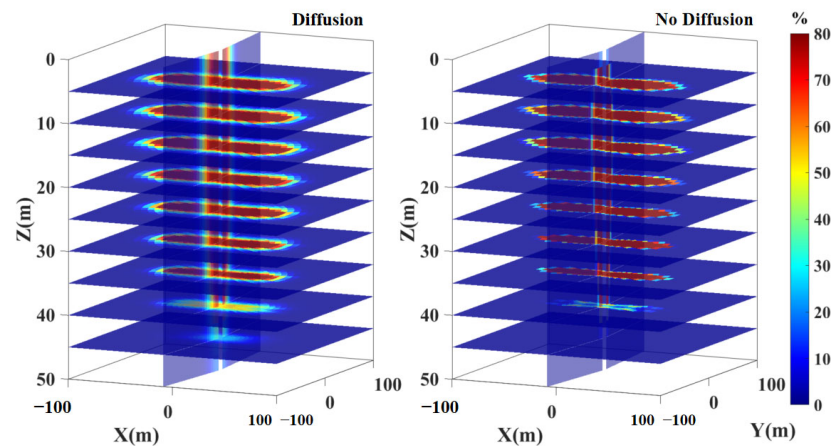


Figure 13. The molar fraction of CO₂ in the third year when the matrix permeability is 1 mD.

4.3. Effect of Radial Borehole Length and Radius

The dimensions of radial boreholes, specifically their length and radius, are critical parameters influenced by the hydraulic aspects of borehole drilling. An increase in the length of a radial borehole directly correlates with a larger reservoir contact area, resulting in a near-linear rise in both oil and gas production. In terms of CO₂ storage, a longer borehole implies an enhanced capacity for both CO₂ injection and production. However, the incremental benefit in CO₂ storage capacity diminishes with increases in borehole length. For instance, as shown in Figure 14, when the radius is fixed at 20 mm and the borehole length is extended from 20 m to 60 m, the oil recovery rate and CO₂ storage rate in the third year increase by factors of 2.15 and 1.27, respectively.

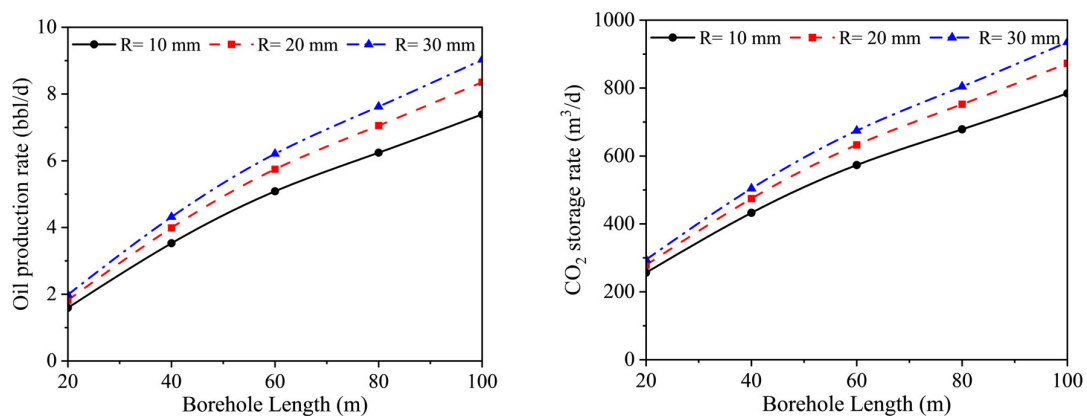


Figure 14. Effects of radial borehole length and diameter on oil production and CO₂ storage.

Conversely, the diameter of the radial borehole, while determining the strength of connectivity between the wellbore and the reservoir, has a relatively subdued impact on productivity compared to borehole length. For example, with a borehole length of 60 m, increasing the borehole radius from 10 mm to 30 mm results in third-year increases of 0.22 and 0.18 times in the oil recovery rate and CO₂ storage rate, respectively.

4.4. Effect of Radial Borehole Branch Number and Phase Angle

The quantity and phase angle of branches in radial boreholes are crucial design parameters for the deployment of multiple radial boreholes. As demonstrated in Figure 15, a greater number of radial boreholes leads to a more uniform distribution of CO₂ injection points. Consequently, an increase in the number of radial boreholes correlates with enhanced oil production and gas storage capabilities. Figure 16 further illustrates that at a phase angle of 0°, increasing the number of radial boreholes from 2 to 4, and then to 6, results in incremental factors of 0.93 and 0.13 in oil production, respectively. This trend suggests that the capacity for CO₂ injection begins to reach saturation beyond four radial boreholes.

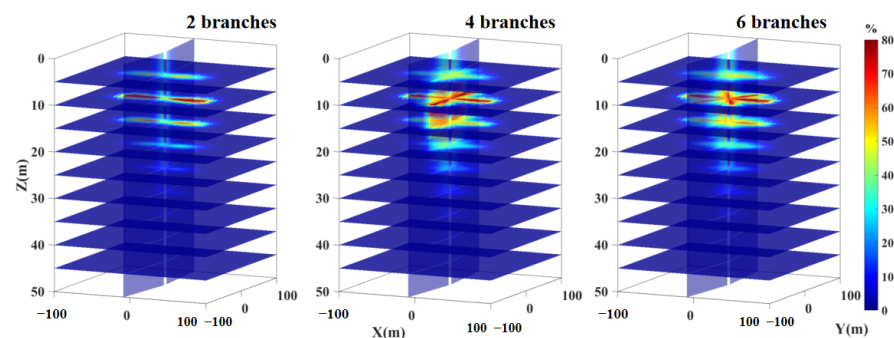


Figure 15. Reservoir CO₂ molar fraction when radial borehole branches are 2, 4, and 6.

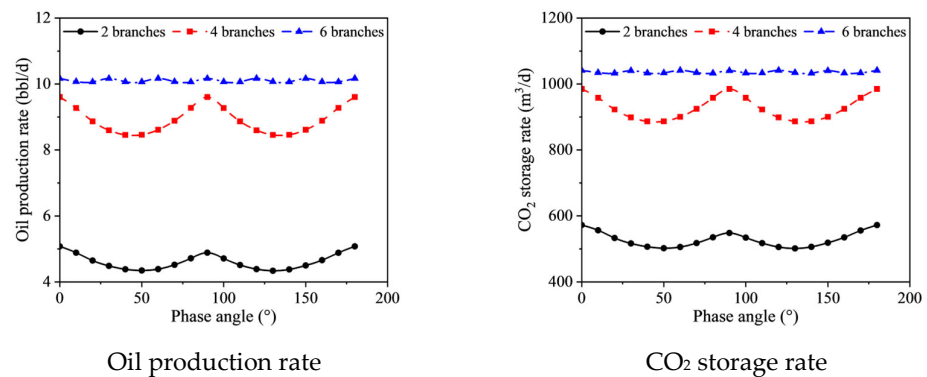


Figure 16. Effects of the number and length of radial borehole branches on oil production rate and CO₂ storage rate.

When the phase angle is small, resulting in a larger pressure differential, each branch of the radial boreholes exhibits increased oil production and greater CO₂ storage capacity. For instance, with a four-branch system, a phase angle of 0° yields an oil production rate 1.14 times higher than that at a phase angle of 40°. However, it is important to note that a higher number of radial boreholes, combined with a phase angle of 0°, can also lead to more pronounced gas channeling in the later stages of CO₂ injection. This increased gas channeling could accelerate the decline in oil production rates. Nonetheless, the detailed analysis of these effects falls outside the scope of this paper.

4.5. Comparison with Horizontal Well Hydraulic Fracturing Methods

In the final part of this paper, the parameters for the four-branch, two-layer radial borehole CO₂-enhanced shale oil development from Section 4.4 are used as a basis to compare with a dual horizontal well CO₂-enhanced shale oil development case. Due to the inability of the embedded discrete fracture method to employ PEBI grids, structured grids were used to compare the oil production of both methods. As shown in Figure 17, the horizontal well fracturing involves a well length of 260 m, which does not directly contact the reservoir. The fracture spacing is 50 m, and other parameters are detailed in Table 3. By calculating the costs using the parameters from Table 3, the cost-efficiency and productivity of both methods are jointly presented in Figure 18. This comparison reveals that, while the productivity of the radial well enhanced shale oil development is only 50.6% of that of the horizontal well fracturing, its cost is merely 11.1% of the latter. Although this is a simplistic comparison, it sufficiently demonstrates that the radial well technology used for enhancing shale oil development is a potent complement to current conventional shale oil development techniques.

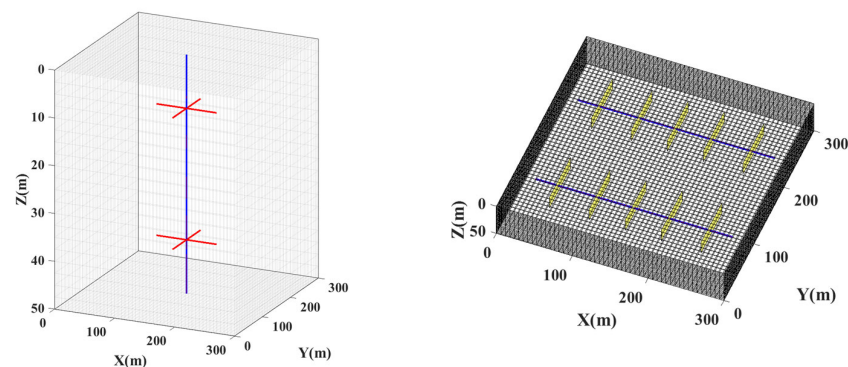
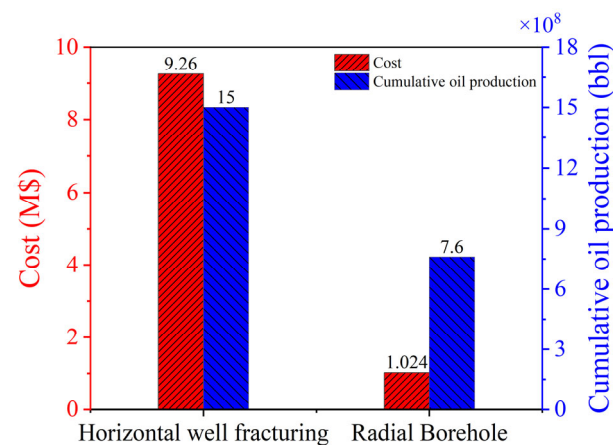


Figure 17. CO₂-enhanced radial well development model for shale oil and dual horizontal well fracturing CO₂-enhanced development (The blue line represents the main well, the red line represents the radial borehole, and the yellow square represents the hydraulic fracture).

Table 3. Drilling and fracturing parameters and prices for radial and horizontal wells [33].

Parameters	Value	Unit
Fracture length	70	m
Fracture height	20	m
Fracture width	0.003	m
Fracture porosity	0.3	
Fracture permeability	200	Darcy
Drilling cost of a horizontal well	2.2	USD M/per
Drilling cost of a vertical well	0.8	USD M/per
Drilling cost of a radial borehole	0.028	USD M/per
Fracturing cost per stage	0.486	USD M/per

**Figure 18.** Comparison of costs and oil production between CO₂-enhanced radial borehole development for shale oil and dual horizontal well fracturing CO₂-enhanced development.

5. Conclusions and Discussions

To address the challenges of high fracturing costs and rapid productivity declines in horizontal shale oil wells, this paper introduces a novel CO₂ enhancement technique for shale oil extraction in radial boreholes. A component numerical simulation methodology was developed, incorporating component diffusion, adsorption, and reservoir fluid non-Darcy flow dynamics, to evaluate the effectiveness of this approach. This study investigates the impact of various parameters including initial reservoir pressure, permeability, radial borehole length and radius, branching number, and phase angle on both oil production and CO₂ storage. Finally, by comparing the production of shale oil enhanced with CO₂ using a four-branch, two-layer radial borehole system with that of a dual horizontal well fracturing system enhanced by CO₂, it was found that although the former's oil production is only 50.6% of the latter, its cost is merely 11.1%, thereby proving its economic viability. The key findings are summarized as follows:

- At a consistent CO₂ injection rate, lower initial reservoir pressures increase the likelihood of immiscible displacement in CO₂-driven crude oil extraction, leading to more rapid CO₂ gas breakthroughs. Consequently, in radial borehole CO₂-enhanced shale oil development, it is recommended to sustain higher initial development or injection pressures to ensure miscible displacement. In scenarios where maintaining the CO₂ injection pressure is challenging, the feasibility of alternate CO₂-N₂ injection methods could be considered, which warrants further investigation in future studies;
- The adsorption of CO₂ in shale oil reservoirs facilitates the release of lighter hydrocarbon components, as it competitively adsorbs these elements. While the diffusion of CO₂ can lead to earlier gas channeling, this effect is counterbalanced by its migration towards areas of lower concentration at the reservoir boundary. This migration, driven not just by the pressure gradient but also by diffusion, results in a reduction in the

extent of CO₂ gas channeling compared to scenarios where diffusion is not taken into account;

- In cases where the reservoir permeability falls below 0.01 mD, the production yield from radial borehole CO₂-enhanced shale oil development is notably low. Hence, it is advisable to select deployment locations within high-permeability “sweet spots” of shale oil reservoirs for this method. To enhance production, employing radial boreholes with greater lengths and larger diameters is beneficial. Alternatively, increasing the number of radial boreholes and adjusting the phase angle to 0° can also be effective strategies;
- In our future work, we will further explore the impact of CO₂-induced asphaltene precipitation, the alteration of surface tension by CO₂, and the hysteresis effects of CO₂ injection on the effectiveness of CO₂-enhanced radial borehole development techniques for shale oil extraction. Additionally, we plan to conduct laboratory experiments and field tests to further substantiate the feasibility of our methods and the precision of our models.

Author Contributions: Conceptualization, S.R., J.D. and T.W.; methodology, J.D.; software, Z.X.; validation, T.W. and K.T.; formal analysis, J.D.; investigation, J.D.; resources, S.T.; data curation, J.D.; writing—original draft preparation, J.D.; writing—review and editing, K.T.; visualization, K.T.; supervision, J.L.; project administration, S.T.; funding acquisition, T.W. All authors have read and agreed to the published version of the manuscript.

Funding: This project is sponsored by the Science Foundation of China University of Petroleum, Beijing (No. 2462023BJRC025), the Open Foundation of Shaanxi Key Laboratory of Lacklustre Shale Gas Accumulation and Exploitation, China University of Petroleum-Beijing 2023 College Student Innovation and Entrepreneurship Training Program Funding (No. D202305271049583327), and the National Science Fund for Distinguished Young Scholars (No. 52204063).

Data Availability Statement: Data is contained within the article.

Acknowledgments: Thanks to the free and open source software MATLAB Reservoir Simulation Toolbox (MRST 2023a) developed by the Computational Geography Group of SINTEF Digital’s Mathematics and Cybernetics Department and other third parties.

Conflicts of Interest: Author Zongan Xue was employed by Oil & Gas Survey, China Geological Survey. The remaining authors declare that the research was conducted in the absence of any commercial or financial relationships that could be construed as a potential conflict of interest.

References

1. Yolcan, O.O. World energy outlook and state of renewable energy: 10-Year evaluation. *Innov. Green Dev.* **2023**, *2*, 100070. [[CrossRef](#)]
2. Tong, X.; Zhang, G.; Wang, Z.; Wen, Z.; Tian, Z.; Wang, H.; Ma, F.; Wu, Y. Distribution and potential of global oil and gas resources. *Pet. Explor. Dev.* **2018**, *45*, 779–789. [[CrossRef](#)]
3. Wang, H.; Ma, F.; Tong, X.; Liu, Z.; Zhang, X.; Wu, Z.; Li, D.; Wang, B.; Xie, Y.; Yang, L. Assessment of global unconventional oil and gas resources. *Pet. Explor. Dev.* **2016**, *43*, 925–940. [[CrossRef](#)]
4. Yang, L.; Jin, Z. Global shale oil development and prospects. *China Pet. Explor.* **2019**, *24*, 553–559.
5. Alfi, M.; Barrufet, M.; Killough, J. Effect of pore sizes on composition distribution and enhance recovery from liquid shale—Molecular sieving in low permeability reservoirs. *Fuel* **2019**, *235*, 1555–1564. [[CrossRef](#)]
6. Chen, C.; Balhoff, M.; Mohanty, K.K. Effect of reservoir heterogeneity on improved shale oil recovery by CO₂ huff-n-puff. In Proceedings of the SPE Unconventional Resources Conference/Gas Technology Symposium, The Woodlands, TX, USA, 4–6 February 2013; p. SPE-164553.
7. Wu, S.; Fang, S.; Ji, L.; Wen, F.; Sun, Z.; Yan, S.; Li, Y. Transport Behavior of Methane Confined in Nanoscale Porous Media: Impact of Pore Evolution Characteristics. *Processes* **2022**, *10*, 2746. [[CrossRef](#)]
8. Yu, H.; Xu, H.; Fu, W.; Lu, X.; Chen, Z.; Qi, S.; Wang, Y.; Yang, W.; Lu, J. Extraction of shale oil with supercritical CO₂: Effects of number of fractures and injection pressure. *Fuel* **2021**, *285*, 118977. [[CrossRef](#)]
9. Zhu, C.; Li, Y.; Zhao, Q.; Gong, H.; Sang, Q.; Zou, H.; Dong, M. Experimental study and simulation of CO₂ transfer processes in shale oil reservoir. *Int. J. Coal Geol.* **2018**, *191*, 24–36. [[CrossRef](#)]
10. Boak, J.; Kleinberg, R. Shale gas, tight oil, shale oil and hydraulic fracturing. In *Future Energy*; Elsevier: Amsterdam, The Netherlands, 2020; pp. 67–95.

11. Xu, Y.; Sheng, G.; Zhao, H.; Hui, Y.; Zhou, Y.; Ma, J.; Rao, X.; Zhong, X.; Gong, J. A new approach for gas-water flow simulation in multi-fractured horizontal wells of shale gas reservoirs. *J. Pet. Sci. Eng.* **2021**, *199*, 108292. [[CrossRef](#)]
12. Zhang, Y.; Zhang, Y.; Zhou, L.; Lei, Z.; Guo, L.; Zhou, J. Reservoir stimulation design and evaluation of heat exploitation of a two-horizontal-well enhanced geothermal system (EGS) in the Zhaocang geothermal field, Northwest China. *Renew. Energy* **2022**, *183*, 330–350. [[CrossRef](#)]
13. Freyman, M. *Hydraulic Fracturing & Water Stress: Water Demand by the Numbers*; Ceres: Boston, MA, USA, 2014.
14. Sanaei, A.; Shakiba, M.; Varavei, A.; Sepehrnoori, K. Mechanistic Modeling of Clay Swelling in Hydraulic-Fractures Network. *SPE Reserv. Eval. Eng.* **2018**, *21*, 96–108. [[CrossRef](#)]
15. Wachtmeister, H.; Lund, L.; Aleklett, K.; Höök, M. Production decline curves of tight oil wells in eagle ford shale. *Nat. Resour. Res.* **2017**, *26*, 365–377. [[CrossRef](#)]
16. Wood, T.; Milne, B. *Waterflood Potential Could Unlock Billions of Barrels: Crescent Point Energy*; Dundee Securities Ltd.: Toronto, ON, Canada, 2011.
17. Ji, Z.; Zhao, J.; Chen, X.; Gao, Y.; Xu, L.; He, C.; Ma, Y.; Yao, C. Three-Dimensional Physical Simulation of Horizontal Well Pumping Production and Water Injection Disturbance Assisted CO₂ Huff and Puff in Shale Oil Reservoir. *Energies* **2022**, *15*, 7220. [[CrossRef](#)]
18. Sheng, J.J.; Chen, K. Evaluation of the EOR potential of gas and water injection in shale oil reservoirs. *J. Unconv. Oil Gas Resour.* **2014**, *5*, 1–9. [[CrossRef](#)]
19. Jia, B.; Tsau, J.-S.; Barati, R. A review of the current progress of CO₂ injection EOR and carbon storage in shale oil reservoirs. *Fuel* **2019**, *236*, 404–427. [[CrossRef](#)]
20. Celia, M.A.; Bachu, S.; Nordbotten, J.M.; Bandilla, K.W. Status of CO₂ storage in deep saline aquifers with emphasis on modeling approaches and practical simulations. *Water Resour. Res.* **2015**, *51*, 6846–6892. [[CrossRef](#)]
21. Celia, M.A. Geological storage of captured carbon dioxide as a large-scale carbon mitigation option. *Water Resour. Res.* **2017**, *53*, 3527–3533. [[CrossRef](#)]
22. Saini, D. *CO₂-Reservoir Oil Miscibility: Experimental and Non-Experimental Characterization and Determination Approaches*; Springer: Berlin/Heidelberg, Germany, 2018.
23. Zhang, K.; Jia, N.; Li, S.; Liu, L. Static and dynamic behavior of CO₂ enhanced oil recovery in shale reservoirs: Experimental nanofluidics and theoretical models with dual-scale nanopores. *Appl. Energy* **2019**, *255*, 113752. [[CrossRef](#)]
24. Wang, R.; Bi, S.; Guo, Z.; Feng, G. Molecular insight into replacement dynamics of CO₂ enhanced oil recovery in nanopores. *Chem. Eng. J.* **2022**, *440*, 135796. [[CrossRef](#)]
25. Li, B.; Zheng, L.; Cao, A.; Bai, H.; Zhang, C.; Li, Z. Effect of interaction between CO₂ and crude oil on the evolution of interface characteristics. *Colloids Surf. A Physicochem. Eng. Asp.* **2022**, *647*, 129043. [[CrossRef](#)]
26. Yang, Z.; Li, M.; Peng, B.; Lin, M.; Dong, Z. Volume expansion of CO₂ + oil at near critical and supercritical conditions of CO₂. *Fuel* **2013**, *112*, 283–288. [[CrossRef](#)]
27. Li, H.; Zheng, S.; Yang, D. Enhanced swelling effect and viscosity reduction of solvent(s)/CO₂/heavy-oil systems. *SPE J.* **2013**, *18*, 695–707. [[CrossRef](#)]
28. Yang, D.; Tontiwachwuthikul, P.; Gu, Y. Interfacial tensions of the crude oil + reservoir brine + CO₂ systems at pressures up to 31 MPa and temperatures of 27 °C and 58 °C. *J. Chem. Eng. Data* **2005**, *50*, 1242–1249. [[CrossRef](#)]
29. Kumar, N.; Sampaio, M.A.; Ojha, K.; Hoteit, H.; Mandal, A. Fundamental aspects, mechanisms and emerging possibilities of CO₂ miscible flooding in enhanced oil recovery: A review. *Fuel* **2022**, *330*, 125633. [[CrossRef](#)]
30. Abedini, A.; Torabi, F. On the CO₂ storage potential of cyclic CO₂ injection process for enhanced oil recovery. *Fuel* **2014**, *124*, 14–27. [[CrossRef](#)]
31. Zhou, X.; Yuan, Q.; Peng, X.; Zeng, F.; Zhang, L. A critical review of the CO₂ huff ‘n’ puff process for enhanced heavy oil recovery. *Fuel* **2018**, *215*, 813–824. [[CrossRef](#)]
32. Stalkup, F. Carbon dioxide miscible flooding: Past, present, and outlook for the future. *J. Pet. Technol.* **1978**, *30*, 1102–1112. [[CrossRef](#)]
33. Dai, J.; Zheng, Z.; Wang, T.; Li, G. Productivity and Cost Comparison between Radial-Borehole Fracturing and Horizontal Well Fracturing in Shale Oil Reservoir. In Proceedings of the Gas & Oil Technology Showcase and Conference, Dubai, United Arab Emirates, 13–15 March 2023; OnePetro: Richardson, TX, USA, 2023.
34. Chase, C.A.; Todd, M.R. Numerical simulation of CO₂ flood performance. *Soc. Pet. Eng. J.* **1984**, *24*, 597–605. [[CrossRef](#)]
35. Edouard, M.N.; Okere, C.J.; Ejike, C.; Dong, P.; Suliman, M.A. Comparative numerical study on the co-optimization of CO₂ storage and utilization in EOR, EGR, and EWR: Implications for CCUS project development. *Appl. Energy* **2023**, *347*, 121448. [[CrossRef](#)]
36. Kim, M.; Kwon, S.; Ji, M.; Shin, H.; Min, B. Multi-lateral horizontal well with dual-tubing system to improve CO₂ storage security and reduce CCS cost. *Appl. Energy* **2023**, *330*, 120368. [[CrossRef](#)]
37. Enab, K.; Ertekin, T. Screening and optimization of CO₂-WAG injection and fish-bone well structures in low permeability reservoirs using artificial neural network. *J. Pet. Sci. Eng.* **2021**, *200*, 108268. [[CrossRef](#)]
38. Li, J.; Huang, Z.; Li, G.; Huang, Z.; Dai, J.; Cheng, K. Field test of radial jet drilling technology in a surface formation. *J. Pet. Sci. Eng.* **2022**, *218*, 110928. [[CrossRef](#)]

39. Blöcher, G.; Peters, E.; Reinsch, T.; Petrauskas, S.; Valickas, R.; van den Berg, S. *D3.2 Report on Radial Jet-Drilling (RJD) Stimulation Technology*; German Research Centre for Geosciences: Postdam, Germany, 2016.
40. Kamel, A.H. A technical review of radial jet drilling. *J. Pet. Gas Eng.* **2017**, *8*, 79–89.
41. Tian, Y.; Xiong, Y.; Wang, L.; Lei, Z.; Zhang, Y.; Yin, X.; Wu, Y.-S. A compositional model for gas injection IOR/EOR in tight oil reservoirs under coupled nanopore confinement and geomechanics effects. *J. Nat. Gas Sci. Eng.* **2019**, *71*, 102973. [[CrossRef](#)]
42. Fussell, L.T.; Fussell, D.D. An iterative technique for compositional reservoir models. *Soc. Pet. Eng. J.* **1979**, *19*, 211–220. [[CrossRef](#)]
43. Zhao, X.; Chen, Z.; Wang, B.; Liao, X.; Li, D.; Zhou, B. A Multi-medium and Multi-mechanism model for CO₂ injection and storage in fractured shale gas reservoirs. *Fuel* **2023**, *345*, 128167. [[CrossRef](#)]
44. Møyner, O.; Tchelepi, H. A multiscale restriction-smoothed basis method for compositional models. In Proceedings of the SPE Reservoir Simulation Conference, Montgomery, TX, USA, 20–22 February 2017; p. D031S009R003.
45. Zhong, Y.; She, J.; Zhang, H.; Kuru, E.; Yang, B.; Kuang, J. Experimental and numerical analyses of apparent gas diffusion coefficient in gas shales. *Fuel* **2019**, *258*, 116123. [[CrossRef](#)]
46. Ambrose, R.J.; Hartman, R.C.; Akkutlu, I.Y. Multi-component sorbed-phase considerations for shale gas-in-place calculations. In Proceedings of the SPE Oklahoma City Oil and Gas Symposium/Production and Operations Symposium, Oklahoma City, OK, USA, 23–26 March 2011; p. SPE-141416.
47. Yang, S.; Wu, K.; Xu, J.; Li, J.; Chen, Z. Roles of multicomponent adsorption and geomechanics in the development of an Eagle Ford shale condensate reservoir. *Fuel* **2019**, *242*, 710–718. [[CrossRef](#)]
48. Wang, X.; Sheng, J.J. Effect of low-velocity non-Darcy flow on well production performance in shale and tight oil reservoirs. *Fuel* **2017**, *190*, 41–46. [[CrossRef](#)]
49. Xu, J.; Wu, K.; Yang, S.; Cao, J.; Chen, Z.; Pan, Y.; Yan, B. Real gas transport in tapered noncircular nanopores of shale rocks. *AIChE J.* **2017**, *63*, 3224–3242. [[CrossRef](#)]
50. Beskok, A.; Karniadakis, G.E. Report: A model for flows in channels, pipes, and ducts at micro and nano scales. *Microscale Thermophys. Eng.* **1999**, *3*, 43–77.
51. Rangarajan, R.; Mazid, M.; Matsuura, T.; Sourirajan, S. Permeation of pure gases under pressure through asymmetric porous membranes. Membrane characterization and prediction of performance. *Ind. Eng. Chem. Process Des. Dev.* **1984**, *23*, 79–87. [[CrossRef](#)]
52. Civan, F. *Porous Media Transport Phenomena*; John Wiley & Sons: Hoboken, NJ, USA, 2011.
53. Civan, F. Effective correlation of apparent gas permeability in tight porous media. *Transp. Porous Media* **2010**, *82*, 375–384. [[CrossRef](#)]
54. Peaceman, D.W. *Fundamentals of Numerical Reservoir Simulation*; Elsevier: Amsterdam, The Netherlands, 2000.
55. Lie, K.-A. *An Introduction to Reservoir Simulation Using MATLAB/GNU Octave: User Guide for the MATLAB Reservoir Simulation Toolbox (MRST)*; Cambridge University Press: Cambridge, UK, 2019.
56. Møyner, O.; Lie, K. *Advanced Modelling with the MATLAB Reservoir Simulation Toolbox (MRST)*; Cambridge University Press: Cambridge, UK, 2021.
57. Yu, W.; Zhang, Y.; Varavei, A.; Sepehrmoori, K.; Zhang, T.; Wu, K.; Miao, J. Compositional simulation of CO₂ huff ‘n’ puff in Eagle Ford tight oil reservoirs with CO₂ molecular diffusion, nanopore confinement, and complex natural fractures. *SPE Reserv. Eval. Eng.* **2019**, *22*, 492–508. [[CrossRef](#)]
58. Li, J.; Wang, M.; Jiang, C.; Lu, S.; Li, Z. Sorption model of lacustrine shale oil: Insights from the contribution of organic matter and clay minerals. *Energy* **2022**, *260*, 125011. [[CrossRef](#)]
59. Peng, Z.; Sheng, J. Diffusion Effect on Shale Oil Recovery by CO₂ Huff-n-Puff. *Energy Fuels* **2023**, *37*, 2774–2790. [[CrossRef](#)]
60. Li, L.; Hao, Y.; Lv, Y.; Wang, C.; Yao, C.; Zhao, Q.; Xiao, P. Experimental investigation on low-velocity seepage characteristics and influencing factors in a shale oil reservoir. *J. Pet. Sci. Eng.* **2020**, *195*, 107732. [[CrossRef](#)]
61. Xu, J.; Wu, K.; Li, R.; Li, Z.; Li, J.; Xu, Q.; Li, L.; Chen, Z. Nanoscale pore size distribution effects on gas production from fractal shale rocks. *Fractals* **2019**, *27*, 1950142. [[CrossRef](#)]

Disclaimer/Publisher’s Note: The statements, opinions and data contained in all publications are solely those of the individual author(s) and contributor(s) and not of MDPI and/or the editor(s). MDPI and/or the editor(s) disclaim responsibility for any injury to people or property resulting from any ideas, methods, instructions or products referred to in the content.